Journal of Engineering Mathematics, Vol. 5, No. 1, January 1971
Wolters-Noordhoff Publishing–Groningen
Printed in the Netherlands

A Time-Dependent Analysis for Quasi-One-Dimensional, Viscous, Heat Conducting, Compressible Laval Nozzle Flows*

G. I. BENISON AND E. L. RUBIN

Polytechnic Institute of Brooklyn, Farmingdale, N.Y. 11735, USA.

(Received March 13, 1970)

SUMMARY

A technique is presented for the numerical solution of quasi-one-dimensional, viscous, heat conducting, compressible Laval nozzle flows. A time-dependent finite difference scheme is used to integrate the unsteady flow equations yielding second-order accurate steady-state solutions. Several features of the shock wave solution are shown and discussed.

1. Introduction

In this paper, we shall calculate the unsteady flow in a convergent-divergent nozzle using a conditionally stable finite difference scheme. The fluid is considered to be viscous, heat conducting, and compressible and the flow is regarded as quasi-one-dimensional; i.e., the nozzle is considered to be long and slender with slowly varying cross-sectional area and small cross-flow velocities. The equation of state for a perfect gas is assumed valid and the ratio of the coefficients of specific heat is assumed to be constant. However, the temperature dependence of the viscosity and heat conductivity are taken into account. The boundary layer is assumed to be thin and thus the outer edge is essentially located at the nozzle wall. For flows with sufficiently high viscosity, disregarding the viscous effects on the nozzle's walls may have an appreciable effect on the results.

To solve problems of this type, one can use either an Eulerian formulation as given here or a Lagrangian one. The Lagrangian calculation has the advantage that it does not smear discontinuities as does the Eulerian. On the other hand, its extension to multi-dimensional problems is probably more complicated.

A calculation of the flow in a divergent duct was made by Crocco [1]. His difference scheme is consistent with the steady-state differential equations but not with the time-dependent ones; and, in addition, he assumes constant viscosity and heat conductivity.

The numerical scheme we use is second-order accurate in space. In Section 4, which contains the numerical results, we shall discuss some limitations of schemes of this type for the solution of the Navier–Stokes equations.

To start the calculation, we specify only the nozzle geometry and the upstream and downstream flow conditions. Integration of the differential equations yields the flow field and shock structure as a function of time.

2. Differential Equations

Consider a convergent-divergent or Laval nozzle of slowly varying cross-sectional flow area $A(x)$ as shown in Fig. 1, where the centerline of the nozzle lies along the x-axis. The velocity components in the x- and y-directions are u and v, respectively; the direction of flow is from left to right. In the quasi-one-dimensional approximation, it is assumed that $\partial/\partial x$ is small, the velocity component v normal to the mean flow direction is small compared to the total velocity, $\partial/\partial y > \partial/\partial x$, and only the average values of the flow variables are considered at each cross

* This research was conducted under the sponsorship of the Office of Naval Research under Contract No. Nonr 839(34), Project No. NR 061–135.

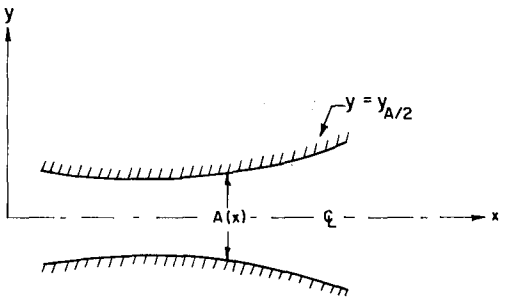

Figure 1. Section of quasi-one-dimensional Laval nozzle.

section. The viscous effects on the nozzle's walls are disregarded. We define the average value of a quantity Q as

$$\bar{Q} = \frac{2}{A}\int_0^{y_{A/2}} Q\,dy\,. \tag{2.1}$$

Neglecting body forces, the unsteady flow of a viscous, heat conducting, compressible fluid may be described by the following set of equations written in Cartesian tensor form using the summation convention:

Continuity:

$$\frac{\partial \rho}{\partial t} + \frac{\partial(\rho u_j)}{\partial x_j} = 0 \tag{2.2a}$$

Momentum:

$$\frac{\partial(\rho u_i)}{\partial t} + \frac{\partial(\rho u_i u_j)}{\partial x_j} = -\frac{\partial p}{\partial x_i} + \frac{\partial \tau_{ik}}{\partial x_k} \tag{2.2b}$$

Energy:

$$\frac{\partial E}{\partial t} + \frac{\partial(E u_j)}{\partial x_j} = -\frac{\partial(p u_j)}{\partial x_j} + \frac{\partial(\tau_{jk} u_j)}{\partial x_k} - \frac{\partial q_k}{\partial x_k} \tag{2.2c}$$

State:

$$p = \rho R T \tag{2.2d}$$

where

$$\tau_{ij} = \mu\left(\frac{\partial u_i}{\partial x_j} + \frac{\partial u_j}{\partial x_i}\right) + (\mu' - \tfrac{2}{3}\mu)\frac{\partial u_l}{\partial x_l}\,\delta_{ij} \tag{2.2e}$$

$$E = \tfrac{1}{2}\rho u^2 + \rho e \tag{2.2f}$$

$$q_j = -k\frac{\partial T}{\partial x_j}\,. \tag{2.2g}$$

Here ρ, u, p and T are the density, velocity, pressure and temperature, respectively. The total energy per unit volume E is the sum of the kinetic energy $\frac{1}{2}\rho u^2$ (we neglect $\frac{1}{2}\rho v^2$ compared to $\frac{1}{2}\rho u^2$) and internal energy ρe. Also, R is the gas constant, k the thermal conductivity, μ the coefficient of viscosity, and μ' is the second coefficient of viscosity, sometimes called the dilatational viscosity, which we take to be zero.

Equations (2.2a), (2.2b), and (2.2c) are now integrated with respect to y from $y=0$ to $y=y_{A/2}$ with the boundary conditions:

$$\text{at } y=0: \quad v=0$$

$$\text{at } y=y_{A/2}: \quad \frac{dy}{dx}=\frac{v}{u}$$

Integrating and applying the usual averaging procedure for small fluctuations from the mean (i.e., such as that used in deriving the governing equations for turbulent flow), we obtain the following three equations consistent with the quasi-one-dimensional approximation:

$$\frac{\partial(\bar{\rho}A)}{\partial t}+\frac{\partial(\bar{\rho}\bar{u}A)}{\partial x}=0 \tag{2.3a}$$

$$\frac{\partial(\bar{\rho}\bar{u}A)}{\partial t}+\frac{\partial(\bar{\rho}\bar{u}\bar{u}A)}{\partial x}=-A\frac{\partial\bar{p}}{\partial x}+\frac{\partial}{\partial x}\left(\tfrac{4}{3}\bar{\mu}\frac{\partial\bar{u}}{\partial x}A\right) \tag{2.3b}$$

$$\frac{\partial(\bar{E}A)}{\partial t}+\frac{\partial(\bar{E}\bar{u}A)}{\partial x}=-\frac{\partial(\bar{p}\bar{u}A)}{\partial x}+\frac{\partial}{\partial x}\left[\left(\tfrac{4}{3}\bar{\mu}\frac{\partial\bar{u}}{\partial x}\right)\bar{u}A\right]+\frac{\partial}{\partial x}\left(\bar{k}\frac{\partial\bar{T}}{\partial x}A\right). \tag{2.3c}$$

Using Eqs. (2.2d) and (2.2f) with $e=c_v T$, we obtain the following two expressions:

$$\bar{p}=(\gamma-1)\left(\bar{E}-\frac{\bar{m}^2}{2\bar{\rho}}\right) \tag{2.4a}$$

$$\bar{T}=\frac{\gamma}{c_p}\frac{\bar{E}}{\bar{\rho}}-\frac{1}{2}\left(\frac{\bar{m}}{\bar{\rho}}\right)^2 \tag{2.4b}$$

where $\gamma=c_p/c_v$ (c_p and c_v are the specific heats at constant pressure and at constant volume, respectively) and $\bar{m}$ is the momentum $\bar{\rho}\bar{u}$. Equations (2.4a) and (2.4b) are used to eliminate $\bar{p}$ and $\bar{T}$ from the system Eqs. (2.3a, b, c).

Introducing a reference length L, velocity U, and density ρ_0, the equations are nondimensionalized by defining the following dimensionless variables:

$$x^*=\frac{x}{L}, \quad t^*=\frac{tU}{L}, \quad u^*=\frac{\bar{u}}{U}, \quad \rho^*=\frac{\bar{\rho}}{\rho_0}$$

$$m^*=\frac{\bar{m}}{\rho_0 U}, \quad E^*=\frac{\bar{E}}{\rho_0 U^2}, \quad A^*=\frac{A}{L^2}.$$

The coefficients of viscosity and heat conductivity are assumed to be proportional to the first power of the temperature:

$$\bar{\mu}=\mu_0 T^*, \quad \bar{k}=k_0 T^*$$

We find from the nondimensionalization that

$$T^*=\gamma(\gamma-1)M_0^2\left[\frac{E^*}{\rho^*}-\frac{1}{2}\left(\frac{m^*}{\rho^*}\right)^2\right]$$

where M_0 is the reference Mach number.

The resulting nondimensionalized equations may then be written in vector form and for convenience, we no longer use stars for the dimensionless variables:

$$w_t=f_x+Ag_x+S_x \tag{2.5a}$$

where the subscript notation for derivatives has been employed, $A=A(x)$, and w is a vector function of x and t

$$w=\begin{pmatrix}\rho A\\ mA\\ EA\end{pmatrix} \tag{2.5b}$$

f and g are given nonlinear vector functions of w, i.e.,

$$f = \begin{pmatrix} -mA \\ -\dfrac{m^2 A}{\rho} \\ -\dfrac{\gamma EmA}{\rho} + (\gamma-1)\dfrac{m^3 A}{2\rho^2} \end{pmatrix} \tag{2.5c}$$

$$g = \begin{pmatrix} 0 \\ -(\gamma-1)\left(E - \dfrac{m^2}{2\rho}\right) \\ 0 \end{pmatrix} \tag{2.5d}$$

and$S$ is given by

$$S = \begin{pmatrix} 0 \\ \dfrac{4}{3Re} A\left(\dfrac{m}{\rho}\right)_x \left\{\gamma(\gamma-1)M_0^2\left[\dfrac{E}{\rho} - \dfrac{1}{2}\left(\dfrac{m}{\rho}\right)^2\right]\right\} \\ \dfrac{1}{Re}\gamma(\gamma-1)M_0^2\left[\dfrac{E}{\rho} - \dfrac{1}{2}\left(\dfrac{m}{\rho}\right)^2\right]\left\{\dfrac{\gamma}{Pr} A\left[\dfrac{E}{\rho} - \dfrac{1}{2}\left(\dfrac{m}{\rho}\right)^2\right]_x + \dfrac{4}{3}\dfrac{m}{\rho} A\left(\dfrac{m}{\rho}\right)_x\right\} \end{pmatrix} \tag{2.5e}$$

where Re and Pr are the Reynolds and Prandtl numbers, respectively.

Note that the system given by Eq. (2.5a) cannot be written in conservation form.

3. Difference Equations and Stability Analysis

The difference equations to be discussed are defined on the half plane $t>0$, $-\infty<x<\infty$, where $\{x_{\pm n}=\pm n\Delta x,\ t_i=t+i\Delta t;\ n,\ i=0, 1, 2, \ldots\}$ define the uniformly spaced net points of the lattice. We call $w_n^t=w(n\Delta x, t+i\Delta t)$ the mesh function which is defined on this lattice and which constitutes an approximation to the solution of the differential equation (2.5a).

Time-dependent difference methods that may be used for the solution of Eq. (2.5a) have been discussed by one of us in [2]. The two-step method used in this calculation is given below:

$$w_{n+\frac{1}{2}}^{t+\Delta t} = \frac{w_{n+1}^t + w_n^t}{2} + \frac{\Delta t}{\Delta x}\left[f_{n+1}^t - f_n^t\right] + \left(\frac{A_{n+1}+A_n}{2}\right)\frac{\Delta t}{\Delta x}\left[g_{n+1}^t - g_n^t\right] + \frac{\Delta t}{\Delta x}\left[S_{n+1}^t - S_n^t\right] \tag{3.1a}$$

$$w_n^{t+\Delta t} = w_n^t + \frac{\Delta t}{2\Delta x}\left[\frac{f_{n+1}^t - f_{n-1}^t}{2} + f_{n+\frac{1}{2}}^{t+\Delta t} - f_{n-\frac{1}{2}}^{t+\Delta t}\right] + A_n\frac{\Delta t}{2\Delta x}\left[\frac{g_{n+1}^t - g_{n-1}^t}{2} + g_{n+\frac{1}{2}}^{t+\Delta t} - g_{n+\frac{1}{2}}^{t+\Delta t}\right] + \frac{\Delta t}{2\Delta x}\left[S_{n+1}^t - S_{n-1}^t\right]. \tag{3.1b}$$

The overall scheme has second-order accuracy.

For the stability analysis, we linearize Eq. (2.5a) by writing

$$w_t = (B+AF+D)w_x + Cw_{xx}$$

where $A=A(x)$ and

$$B = \frac{\partial f}{\partial w},\quad C = \frac{\partial S}{\partial w_x},\quad D = \frac{\partial S}{\partial w},\quad F = \frac{\partial g}{\partial w}.$$

We regard A and the matrices B, C, D, and F as locally constant for purposes of the stability investigation and see under what conditions the eigenvalues of the amplification matrix are in magnitude less than one. In effect, we examine the equations for stability at a fixed point in the nozzle. The matrices B, C, D, and F for the nondimensionalized equations are given explicitly as follows:

$$B = \begin{pmatrix} 0 & -1 & 0 \\ -\dfrac{(\gamma-3)m^2}{2\rho^2} & (\gamma-3)\dfrac{m}{\rho} & -(\gamma-1) \\ \dfrac{\gamma E m}{\rho^2} - \dfrac{(\gamma-1)m^3}{\rho^3} & -\dfrac{\gamma E}{\rho} + \dfrac{3(\gamma-1)m^2}{2\rho^2} & -\dfrac{\gamma m}{\rho} \end{pmatrix}$$

$$C = \begin{pmatrix} 0 & 0 & 0 \\ -c_1 \dfrac{m}{\rho^3}\left[E - \dfrac{m^2}{\rho}\right] & \dfrac{c_1}{\rho^2}\left[E - \dfrac{m^2}{2\rho}\right] & 0 \\ -\dfrac{1}{\rho^3}\left[E - \dfrac{m^2}{2\rho}\right]\left[c_2\left(E - \dfrac{m^2}{\rho}\right) + c_1\dfrac{m^2}{\rho}\right] & (c_1-c_2)\dfrac{m}{\rho^3}\left[E - \dfrac{m^2}{2\rho}\right] & \dfrac{c_2}{\rho^2}\left[E - \dfrac{m^2}{2\rho}\right] \end{pmatrix}$$

$$F = \begin{pmatrix} 0 & 0 & 0 \\ -\dfrac{(\gamma-1)m^2}{2\rho^2} & (\gamma-1)\dfrac{m}{\rho} & -(\gamma-1) \\ 0 & 0 & 0 \end{pmatrix}$$

We list the elements of the D matrix below, where d_{ij} is the element of the ith row and the jth column:

$$d_{11} = d_{12} = d_{13} = 0$$

$$d_{21} = \frac{c_1}{\rho^3}\left\{\frac{m}{\rho}\left[3E - \frac{2m^2}{\rho}\right]\rho_x + \left[\frac{3m^2}{2\rho} - 2E\right] m_x\right\}$$

$$d_{22} = \frac{c_1}{\rho^3}\left\{\left[\frac{3m^2}{2\rho} - E\right]\rho_x - m m_x\right\}$$

$$d_{23} = \frac{c_1}{\rho^2}\left\{-\frac{m}{\rho}\rho_x + m_x\right\}$$

$$d_{31} = \frac{c_2}{\rho^3}\left\{\frac{1}{\rho}\left[3E^2 - \frac{6Em^2}{\rho} + \frac{5m^4}{2\rho^2}\right]\rho_x + \frac{m}{\rho}\left[3E - \frac{2m^2}{\rho}\right]m_x + \left[\frac{3m^2}{\rho} - 2E\right]E_x\right\} + \frac{c_1}{\rho^4}\left\{\frac{m^2}{\rho}\left[4E - \frac{5m^2}{2\rho}\right]\rho_x + m\left[\frac{2m^2}{\rho} - 3E\right]m_x\right\}$$

$$d_{32} = \frac{c_2}{\rho^3}\left\{\frac{m}{\rho}\left[3E - \frac{2m^2}{\rho}\right]\rho_x + \left[\frac{3m^2}{2\rho} - E\right]m_x - mE_x\right\} + \frac{c_1}{\rho^3}\left\{\frac{m}{\rho}\left[\frac{2m^2}{\rho} - 2E\right]\rho_x + \left[E - \frac{3m^2}{2\rho}\right]m_x\right\}$$

$$d_{33} = \frac{c_2}{\rho^2}\left\{\frac{1}{\rho}\left[\frac{3m^2}{2\rho} - 2E\right]\rho_x - \frac{m}{\rho}m_x + E_x\right\} + c_1\frac{m}{\rho^3}\left\{-\frac{m}{\rho}\rho_x + m_x\right\}.$$

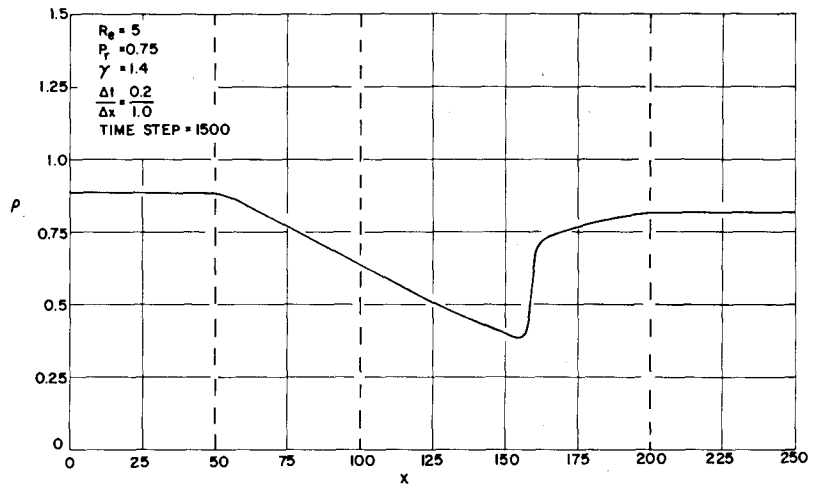

(a) DENSITY DISTRIBUTION

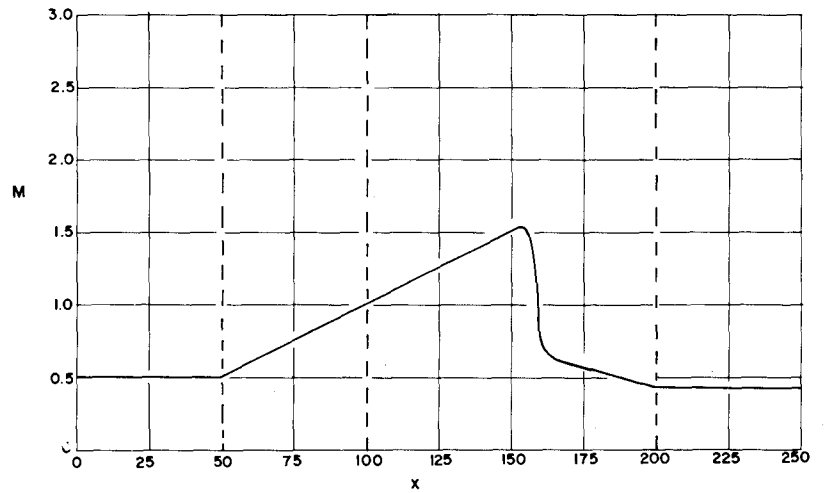

(b) MACH NUMBER DISTRIBUTION

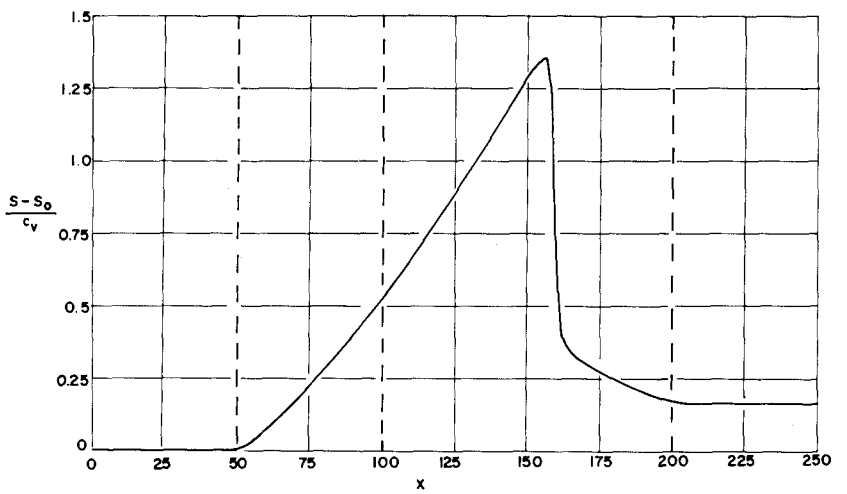

(c) ENTROPY DISTRIBUTION

Figure 2. Distributions of variables in converging-diverging nozzle with shock.

The constants c_1 and c_2 are given by

$$c_1 = \frac{4\gamma(\gamma-1)M_0^2}{3Re} \qquad c_2 = \frac{\gamma^2(\gamma-1)M_0^2}{Re\,Pr}$$

Note, however, that each term of matrix D involves a first derivative of the dependent variables. Then for smoothly varying solutions, the matrix D may be neglected as compared to B and F for the stability analysis. The linearized form that we consider is

$$w_t = (B+AF)w_x + Cw_{xx}\,.$$

The amplification matrix G for system (3.1) is given by

$$G = I + \lambda^2(\cos\xi - 1)(B+AF)^2 + 2\varepsilon(\cos\xi - 1)C$$
$$+ i\{\lambda(\sin\xi)(B+AF) + \lambda\varepsilon(\sin\xi\cos\xi - \sin\xi)(B+AF)C\}$$

where I is the unit matrix, $\xi = l\Delta x$, $\lambda = \Delta t/\Delta x$, and $\varepsilon = \Delta t/(\Delta x)^2$.

Calculation showed that it was always possible to find values of Δt such that the magnitude of the complex eigenvalues of G were less than one. The linearized version of the difference scheme is therefore stable.

4. Numerical Results

In the calculations, the computing region extends from $x=0$ to $x=250$. The convergent section of the Laval nozzle is located between $x=50$ and $x=100$ and the divergent section between $x=100$ and $x=200$ with constant area sections in the remaining regions. The nozzle throat is located at $x=100$. The cross-sectional area $A(x)$ decreases from 1.340 to 1.000 in the convergent section and increases to 1.668 in the divergent section. Throughout the calculations we take $\gamma=1.4$ and use the upstream end conditions as the reference state.

The boundary conditions are prescribed as follows. At the upstream end ($x=0$, 1), we require that conditions stay at their initial values:

$$w_0^{t+\Delta t} = w_1^{t+\Delta t} = w_0^t\,. \tag{4.1}$$

The downstream boundary condition ($x=249$, 250) determines the shock location. Since the solution must be allowed to adjust to its proper value, we fix the density but let the other variables adjust; i.e., we prescribe:

$$\rho_{249}^{t+\Delta t} = \rho_{250}^{t+\Delta t} = \rho_{250}^t\,, \quad m_{249}^t = m_{250}^t = m_{248}^t\,, \quad E_{249}^t = E_{250}^t = E_{248}^t\,.$$

For our first calculation, we considered a shock standing in the divergent section at $x=160$. The initial conditions were calculated from the usual one-dimensional, inviscid isentropic flow relations on both sides of the shock and the Rankine–Hugoniot relations were used across it. Figure 2 shows the results at time step 1500 for a Reynolds number of 5 and a Prandtl number of $\frac{3}{4}$. The density (Fig. 2a) decreases with x in the convergent section and continues to do so in the divergent section up to the shock. Across the shock, the density increases sharply and continues to increase gradually in the remainder of the divergent section. The Mach number distribution (Fig. 2b) shows that the subsonic flow in the convergent section is accelerated to sonic velocity at the throat and is further accelerated supersonically in the divergent section up to the shock. The flow becomes subsonic across the shock and decelerates in the remainder of the divergent section. A specification of the boundary conditions at the nozzle ends is sufficient to maintain a Mach number of unity at the throat. The pressure at the throat is 0.528 which is the value obtained from the quasi-one-dimensional Laval nozzle equations for isentropic flow. The entropy (Fig. 2c) has a maximum since in the tail of the shock the time rate of heat loss by conduction exceeds the rate at which heat is gained by viscous dissipation, resulting in a decrease of entropy.

The results are shown for $\Delta t/\Delta x = 0.2/1.0$ which differs by less than 1% at corresponding points from a mesh of twice that size.

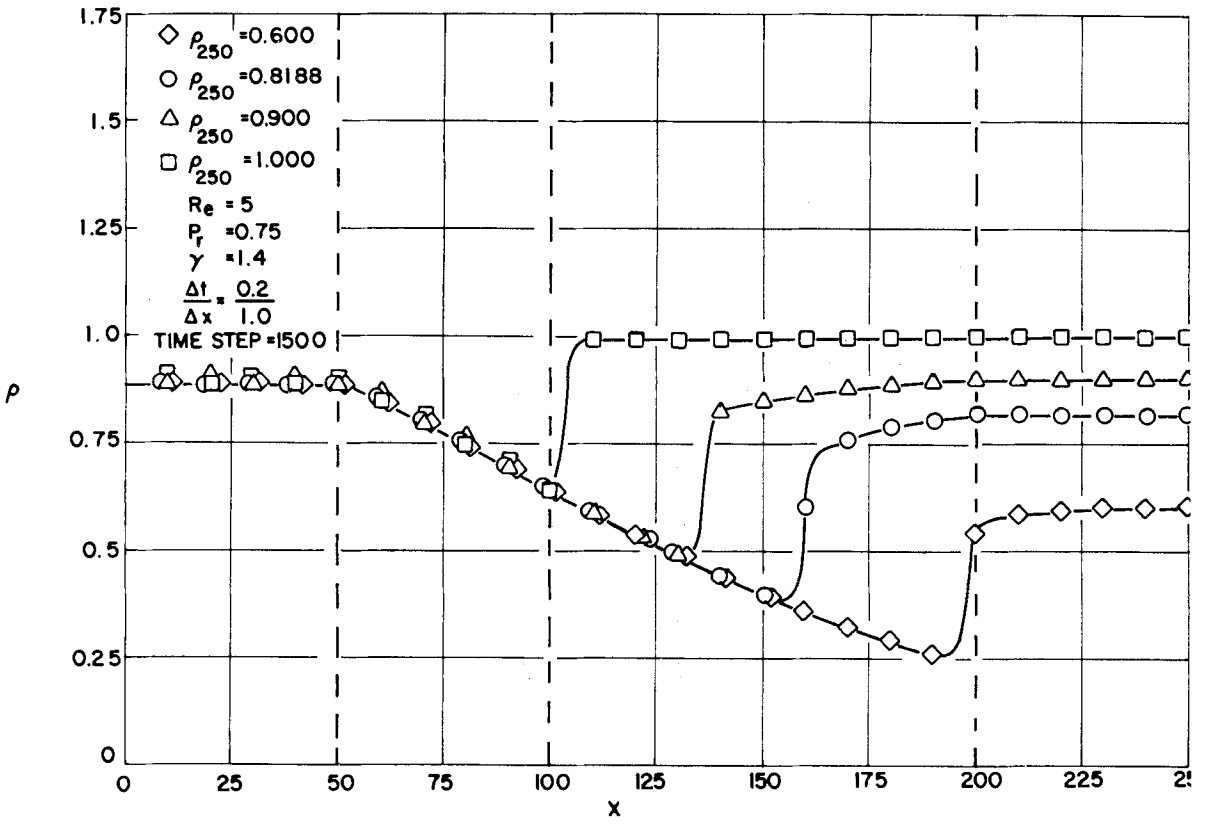

(a) VARIATION OF DENSITY IN THE NOZZLE

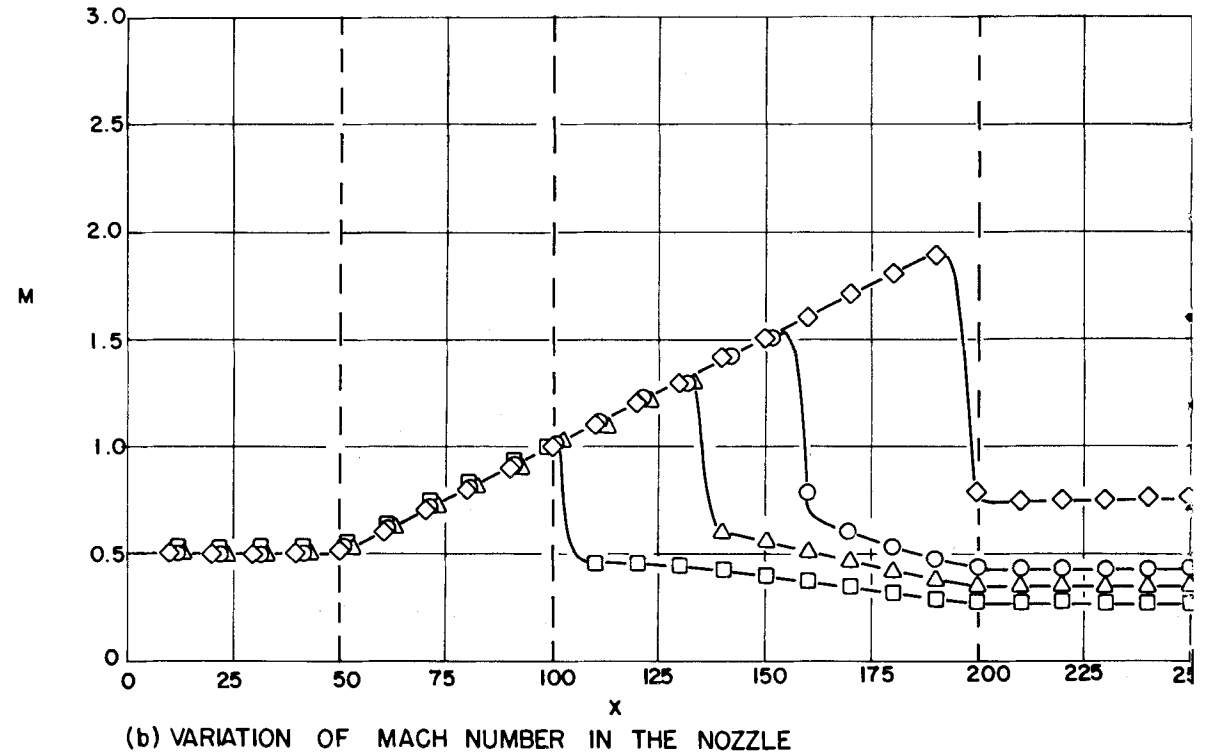

(b) VARIATION OF MACH NUMBER IN THE NOZZLE

Figure 3. Performance curves of converging-diverging nozzle with various downstream conditions.

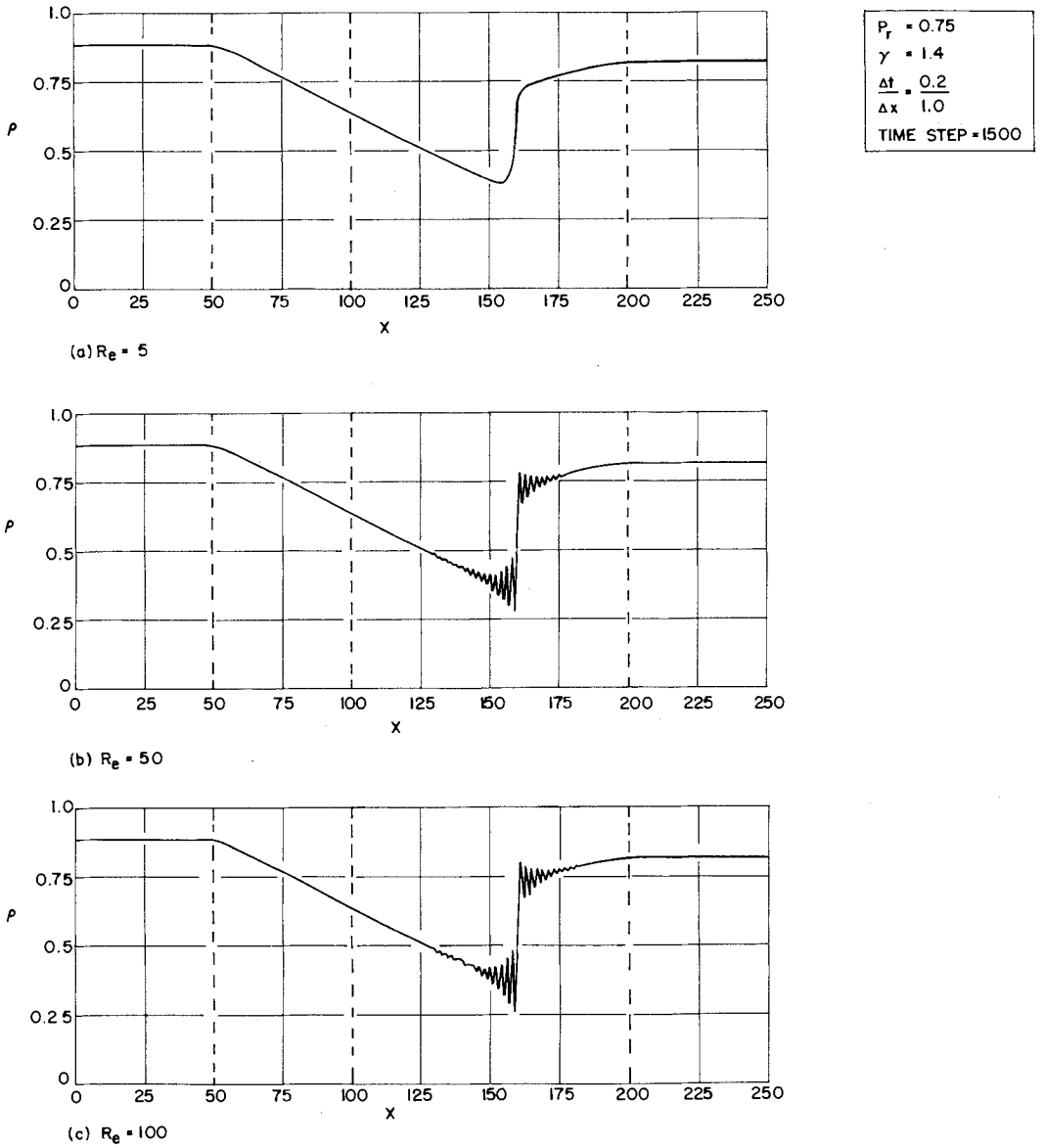

Figure 4. Density distribution for increasing Reynolds number.

To see if the numerical scheme could generate a discontinuous solution from continuous initial data, we prescribed the previously used upstream and downstream conditions at the end points of the nozzle subject to the boundary conditions (4.1) upstream and (4.2) downstream. The initial distributions of ρ, m, and E in the nozzle were taken to vary linearly between the end conditions. The proper discontinuity and flow field appears but requires a longer computational time for convergence.

We next considered the behavior of a standing shock solution with varying downstream density with the purpose of simulating a variation in back pressure. Figure 3 shows the density and Mach number distributions at time step 1500 for a Reynolds number of 5 and a Prandtl number of $\frac{3}{4}$ with various downstream conditions. The curves for $\rho_{250}=0.8188$ correspond to the curves shown in Fig. 2. Decreasing the value of ρ_{250} moves the shock downstream. As the value of ρ_{250} is increased, the shock moves upstream, and for $\rho_{250}=1.0000$ the shock is shown to stand slightly downstream of the throat. However, at time step 1500 the solution for

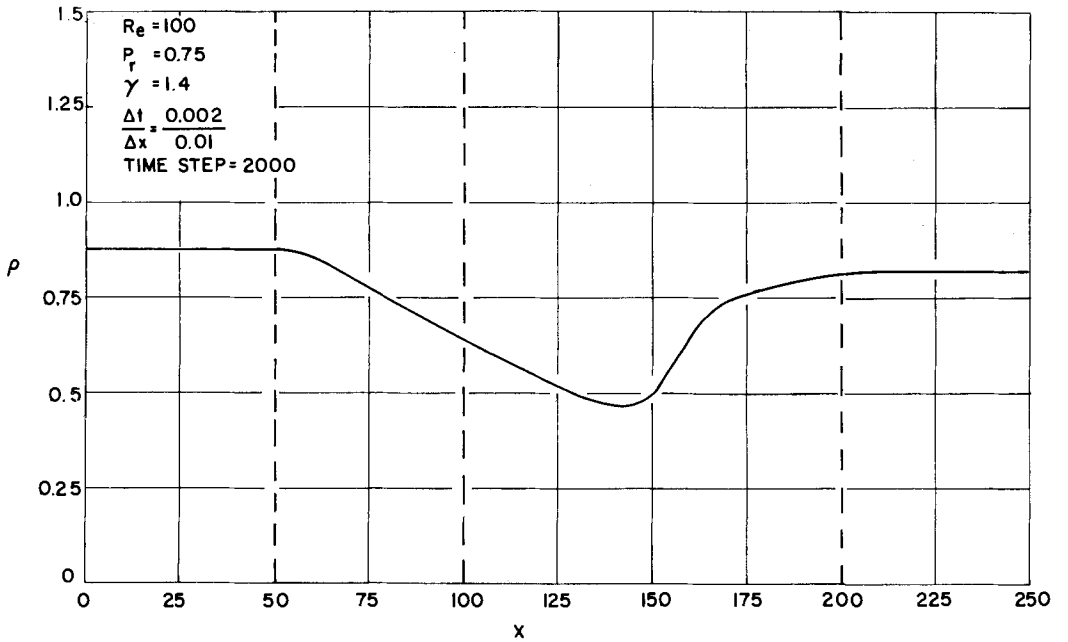

Figure 5. Smooth density distribution for high Reynolds number ($Re=100$) with $\Delta x=1/Re$.

$\rho_{250}=1.0000$ had not yet converged and further integration in time would be required to yield the expected subsonic shockfree solution.

Variations in the Prandtl number yield only slight changes in the flow field. For all values of Pr greater than $\frac{3}{4}$ the results remain virtually unchanged.

For higher Reynolds numbers, a wavy pattern appears on either side of the shock as shown in Fig. 4. By choosing $\Delta x=1/Re$, the results are smooth for the higher Reynolds numbers (Fig. 5) but the shock is now considerably smeared out. We believe this wavy pattern results for the higher Reynolds numbers because the effect of the physical viscosity terms in the equations become small and the equations approach those of inviscid hydrodynamics which are hyperbolic in character. For these equations, the existence of the oscillations is well-known. They have been observed experimentally by Crocco [1] and Rubin and Burstein [2] and Kreiss [4, 5] has shown them to be expected on theoretical grounds also. In spite of the wavy behavior of the solution, a sharp shock is rather well defined (Fig. 4). On the other hand, choosing $\Delta x=1/Re$ leads to unrealistic shock thicknesses as observed in Fig. 5. This difficulty arises because there are two characteristic distances in the problem, i.e., the hydrodynamic distance based on the nozzle length and the shock distance based on the mean free path of the gas.

The use of a technique of this type for the solution of multi-dimensional viscous, heat conducting, compressible flow problems has the advantage that only the specification of the flow geometry and initial and boundary conditions is required. The appearance or non-appearance of shocks arises automatically on numerical integration of the equations and no *a priori* specification is required. Because of the existence of two characteristic lengths in the problem and the use of the hydrodynamic length as the unit of distance in the numerical calculation, there will be a physically unrealistic smearing of all shocks. The overall accuracy of the scheme, however, will still be second-order.

REFERENCES

[1] L. Crocco, A Suggestion for the Numerical Solution of the Steady Navier–Stokes Equations, *AIAA Journal*, 3, 10 (1965) 1824–1832.

[2] E. L. Rubin and S. Z. Burstein, Difference Methods for the Inviscid and Viscous Equations of a Compressible Gas, *Journal of Computational Physics*, 2, 2 (1967) 178–196.

[3] M. Morduchow and P. A. Libby, On the Distribution of Entropy Through a Shock Wave, *Journal de Mécanique*, 4, 2 (1965) 191–213.
[4] H. O. Kreiss and O. Widlund, *Difference Approximations for Initial Value Problems for Partial Differential Equations*, Uppsala University Report No. NR 7, September (1967) 65–70.
[5] H. O. Kreiss and E. Lundqvist, On Difference Approximations with Wrong Boundary Values, *Mathematics of Computation*, 22, 101 (1968) 1–12.

Journal of Engineering Math., Vol. 5 (1971) 39–49